Research Article

Examining Fluvial Stratigraphic Architecture Using Ground-Penetrating Radar at the Fanta Stream Fossil and Archaeological Site, Central Ethiopia

Peter Lanzarone,[1,*,†] Ervan Garrison,[1] René Bobe,[2] and Assiged Getahun[3]

[1]Department of Geology, The University of Georgia, Athens, Georgia
[2]Departamento de Anthropología, Universidad de Chile, Santiago, Chile
[3]Department of Regional Geology and Geochemistry, Geological Survey of Ethiopia, Addis Ababa, Ethiopia

Correspondence
*Corresponding author; E-mail: planzarone@gmail.com

Received
27 March 2014
Revised
22 December 2015
Accepted
2 January 2016

†Current affiliation: BP America.
Scientific editing by Jamie Woodward

Published online in Wiley Online Library (wileyonlinelibrary.com).

doi 10.1002/gea.21584

The Fanta Stream site is an archaeological and paleontological locality in Addis Ababa, Ethiopia. The site contains a rich assemblage of fossil mammals and Acheulean artifacts of approximately 600 ka located in a rare high-altitude context. A ground-penetrating radar (GPR) survey was conducted in order to provide three-dimensional imaging of the subsurface, which the authors use to interpret the geometry and distribution of fossil-containing stratigraphic units. Utilizing the stream's natural cut bank exposure, we calibrate GPR data to known geologic units through radar facies analysis. Shallow, high-amplitude coherent reflection geometries are attributed to volcanic tuff deposits, as these units exhibit subparallel continuous reflections consistent with planar stratified sedimentary deposition. Deeper, discontinuous reflection packages are interpreted as conglomeritic, fossil-containing deposits. The results of the GPR survey outline the location of the Fanta Stream's paleodepositional features as well as suggest the extent of fossiliferous stratigraphic units for use in future excavations.

INTRODUCTION

Ethiopia has long been noted for its importance as a paleoanthropological hotspot where significant early hominid discoveries have been made. Emerging technologies in shallow geophysics have enabled the identification and description of archaeological sites throughout much of the world and many researchers are embracing these techniques. However, shallow geophysical technologies remain underutilized at East African fossil and archaeological sites. This may be due to the remoteness of fossil localities, logistical issues, or the lack of prior studies in the region. Despite this, there is clearly an advantage to acquire geophysical data to help describe unexcavated portions of a site or aid in the identification of new sites.

Ground-penetrating radar, GPR, has been applied to archaeological contexts since the late 1970s, although little published material has explored the application of GPR in identifying the extent of fossil-rich deposits (with one of the earliest papers by Main & Hammond, 2003). In our study, GPR was selected as an appropriate geophysical tool to evaluate the extent of fluvial deposits in our study area, most notably for its utility in guiding excavations and providing non-destructive analyses (Sharma, 2002; Garrison, 2003; Kvamme, 2003; Conyers, 2004). GPR studies used to characterize fluvial stratigraphic environments (e.g., Leclerc & Hicken, 1997; Skelly, Bristow, & Ethridge, 2003; Patidar et al., 2007) as well as geoarchaeological studies within fluvial contexts have also been long demonstrated (e.g., Słowik, 2010; Wright et al., 2014).

This paper describes GPR analyses conducted at the Fanta Stream paleontological and archaeological site in Addis Ababa, Ethiopia. The site has had limited evaluation despite its importance as potentially one of the most significant accumulations of mammalian fossils and Acheulean (~600 ka) lithic artifacts (Figure 1) outside of the Rift Valley. Paleoanthropological sites are common within the East African Rift Valley where fossil and artifact preservation are more favorable with dense sediment accumulation common in lower elevation settings. Fanta is one of the few sites of its kind outside the Rift Valley in a high-altitude context. The proximity of the Fanta

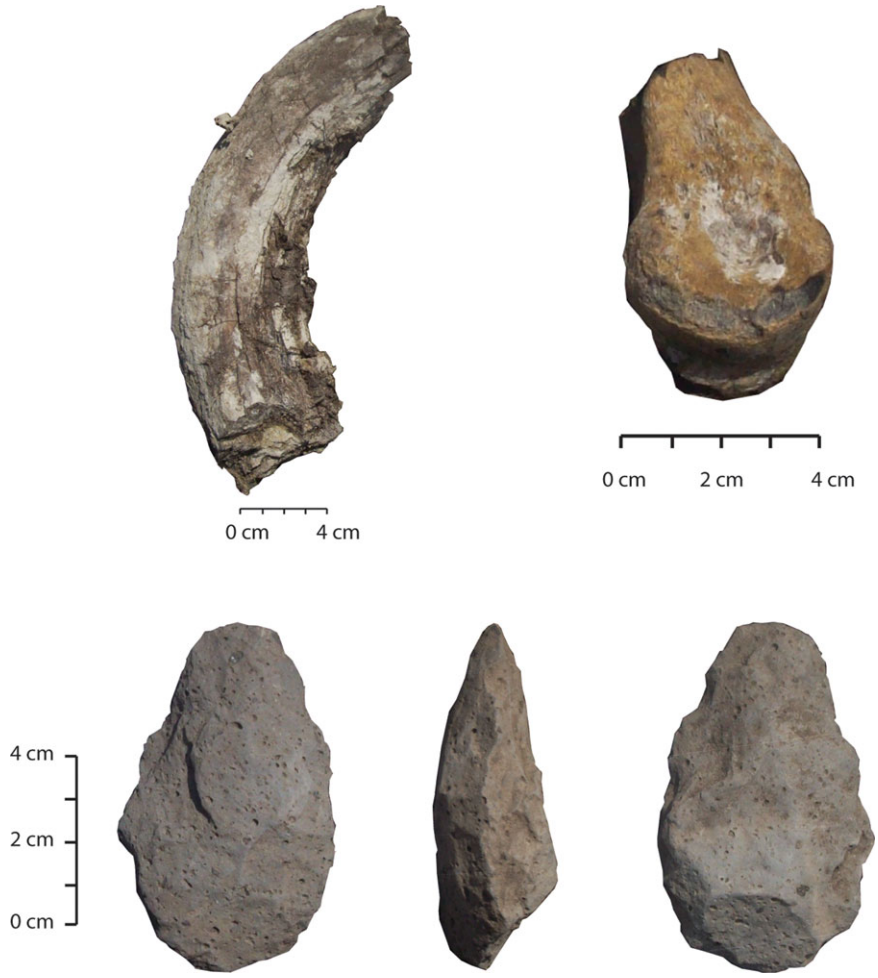

Figure 1 Fossils and lithic artifacts identified during surface reconnaissance at the site. *Hippopotamus*, Bovidae, and *Equus* taxa as well as bifacial hand axes are commonly observed at Fanta, where a small collection of fossil and cultural objects are currently curated at the National Museum of Ethiopia in Addis Ababa.

Stream to the center of Addis Ababa makes the site potentially attractive for visitors and tourists. The Fanta Stream site could provide a unique opportunity for students and the general public to experience paleontological and archaeological research if proper excavation of the site is performed and a museum is established.

At the time of writing, the site is threatened by water drilling projects that began in 2008 and local ongoing agricultural practices. Surface plowing has destroyed fossils and disturbed the sedimentary fidelity with which to study paleoenvironments. Additionally, the area is rich in geological resources where mining for local basalt, pumice, and clay soils are used for road and house construction, household materials, and brick production taking place only a few hundred meters away from the site, posing a danger to the cultural and natural resources at Fanta.

Fossil materials observed in the modern stream's cut bank are unknown at any given distance away from this exposure. Artifacts and fossils that appear at the surface of the site provide some control over characterizing the site's size and geometry, but it is unknown what lies beneath observed surficial deposits. Lithic materials, including Acheulean bifacial handaxes and cleavers have been identified at the site's surface, but not as *in situ* deposits as fossil material have been observed. The principal objective of this study is to delineate the horizontal and vertical distribution of sedimentary units, which the authors can use to predict the extent of fossils and possible artifacts across the site for future protection. We focus on selected GPR transects and depth slices to examine fluvial stratigraphic architecture by correlating radar facies with sedimentary units identified at the site. GPR surveys were conducted across two field seasons, in 2009

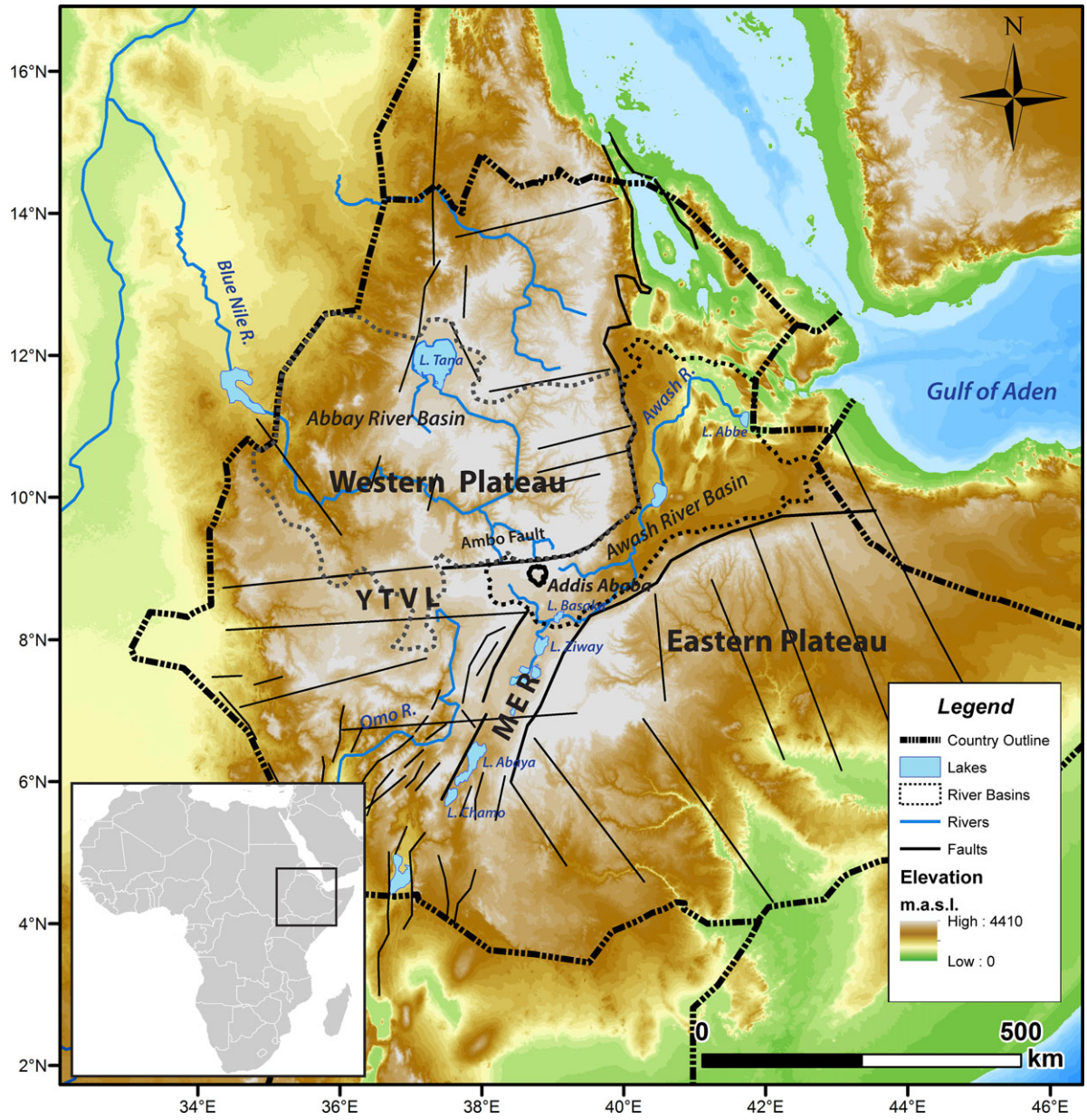

Figure 2 Digital elevation model (DEM) of Ethiopia highlighting major structural and physiographic features that place Addis Ababa and the Fanta Stream site into a regional geologic and geomorphic context. Source: NOAA ETOPO1 Global Relief Map (Amante & Eakins, 2009).

and 2010; however only the results of the 2009 survey are presented here.

STUDY AREA

The geology of Addis Ababa and the region immediately surrounding the Fanta Stream site is the result of the intersection of structural features known collectively as the Main Ethiopian Rift (MER), and the east–west trending fault system known as the Yerer-Tullu Wellel Volcanic Lineament (YTVL) (Figure 2). The YTVL intersects the MER to the west of Addis Ababa, bound at the northern fault margin known as the "Ambo fault." The southern limit of the YTVL is represented as a series of lineaments segmented by NW-SE trending fault systems (Abebe et al., 1998; Boccaletti et al., 1998; Abebe, Balestrieri, & Bigazzi, 2010). Most major rivers follow the NW-SE fault trend, where drainage patterns are controlled by rift shoulder uplifted topography, predominant fracture systems, and central volcanoes (Adhana, 2014).

The Awash River originates from highlands of central Ethiopia and is the most utilized and well-developed river basin in the country. It flows southeast for ~250 km until it enters the Great Rift Valley, following the valley for the rest of its journey to Lake Abe near the border with Djibouti, covering the country's second largest catchment area at nearly ~113,000 km^2 (Hailemariam, 1999; Awulachew et al., 2007). The largest river basin in Ethiopia is the Blue Nile, or "Abbay" River that originates in Lake Tana, the well-known source of the Nile, to eventually converge with the White Nile to form the Nile proper.

The Fanta Stream site surrounds the banks of the Fanta Stream, located within the city limits of Addis Ababa (8°52′56.82″N, 38°48′2.48″E). To the south lies the border of the neighboring city, Akaki. Fanta belongs to the Awash River catchment area, where its position on the western Ethiopian plateau facilitates drainage northeastwards by the Awash River drainage system. Unlike most major rivers that flow away from the rift due to abnormally uplifted rift margins, the Awash river flows into the rift as the YTVL dissects the rift shoulder east of Addis Ababa (Adhana, 2014).

Addis Ababa and the Fanta Stream site sit on the western Ethiopian plateau margin, where Quaternary bedrock and a succession of fluvial and lacustrine sediments comprise the local geology of the study area. At the base of the Fanta Stream site is a complex of Quaternary "Bishoftu" basaltic bedrock, observed in nearby bouldered outcroppings forming a ridge to the south of the site. In the Akaki area, the basalt units are highly vesicular, filled with secondary zeolite and quartz. These are characteristically alkaline and represent Plio-Pleistocene basalt flows associated with well-preserved scoria cones found on the escarpment of the MER south of Addis Ababa (Getahun, 2007).

Overlying the basement rock in the region are lacustrine beds interbedded with Plio-Pleistocene pyroclastic deposits. The basal sedimentary unit above bedrock at the Fanta Stream site is a dense fossil-containing deposit composed of conglomeritic material. This unit is primarily redeposited conglomeritic sandstone to fine-grained sandstone and is observed as a coarsening upward sedimentary package. The clasts are largely composed of basalt and scoriaceous basalt in pebble and cobble form. Locally, the conglomeritic unit is well sorted with variable bedding and coarsely laminated structure.

Volcanic tuffs overlie fossil-containing conglomerates. Tuffs are whitish pink to gray in color and are composed of rock fragments ranging in size from boulders to pebbles, and contain pumices within a matrix of dominant fine-grained sanidine crystals and glass. The rock is friable and exhibits an overall planar laminated structure.

Shallower, gravel deposits contain sedimentary features similar to the conglomeratic section, and are made up of a significant concentration of fossil mammals. This unit is coarse gained with interbedded volcanic materials throughout. Vertisols, commonly called black cotton soils, form the modern landscape at Fanta and range in thickness in the stream cut bank from ~0.25 to 1 m thick. These are shrink-swell clays, where local mud cracks are observed on the site's surface.

The Fanta Stream is surrounded by farmland populated by local residents. Rural inhabitants are dependent on cattle and dry farming a variety of crops such as maize, tef, wheat, and sorghum. The topography of the site is gently rolling, where small, submeter scale topographic variations are often related to seasonal plowing, and less significant relief caused by subsurface structural variation. Figure 3 shows surficial conditions during the GPR survey and exposed stratigraphic units at Fanta where sedimentary and fossiliferous deposits were observed in the modern stream cut bank.

The climate of the area is largely determined by the annual movement of air currents across the country, specifically, the Atlantic equatorial westerlies and the Indian Ocean southerly and easterly currents (Yitbarek et al., 2012). For the escarpment and Rift Valley floor, climate is arid to semiarid. The main rainfall, known locally as "Kiremt," is experienced from June to September when moist winds converge over the Ethiopian highlands. These summer rains account for 65–69% of total annual rainfall (Segele & Lamb, 2005), where a relatively dry season follows for 4 months until the end of January, and a short rain season from February until the end of April occurs. Annual rainfall in the rift floor to the escarpment ranges from 950 to 1090 mm, where the mean annual temperature ranges from 13°C to 20°C (Sagri et al., 2008).

METHODOLOGY

GPR relies on the propagation of electromagnetic (EM) waves, generally between frequencies of 10 and 1500 megahertz (MHz). This frequency range lies within the same segment of the EM spectrum as FM radio, television, and communication devices (Conyers, 2004). Energy used in transmitting EM pulses derive from a trigger generated inside a GPR control unit that is directed through a cable and into an antenna, where a copper plate or wire produces an applied oscillating electrical current. Radar reflections occur at the interface of two dielectrically contrasting materials, the degree of which is related to the relative amplitudes of reflected waves. Observed reflections are created by changes in electrical

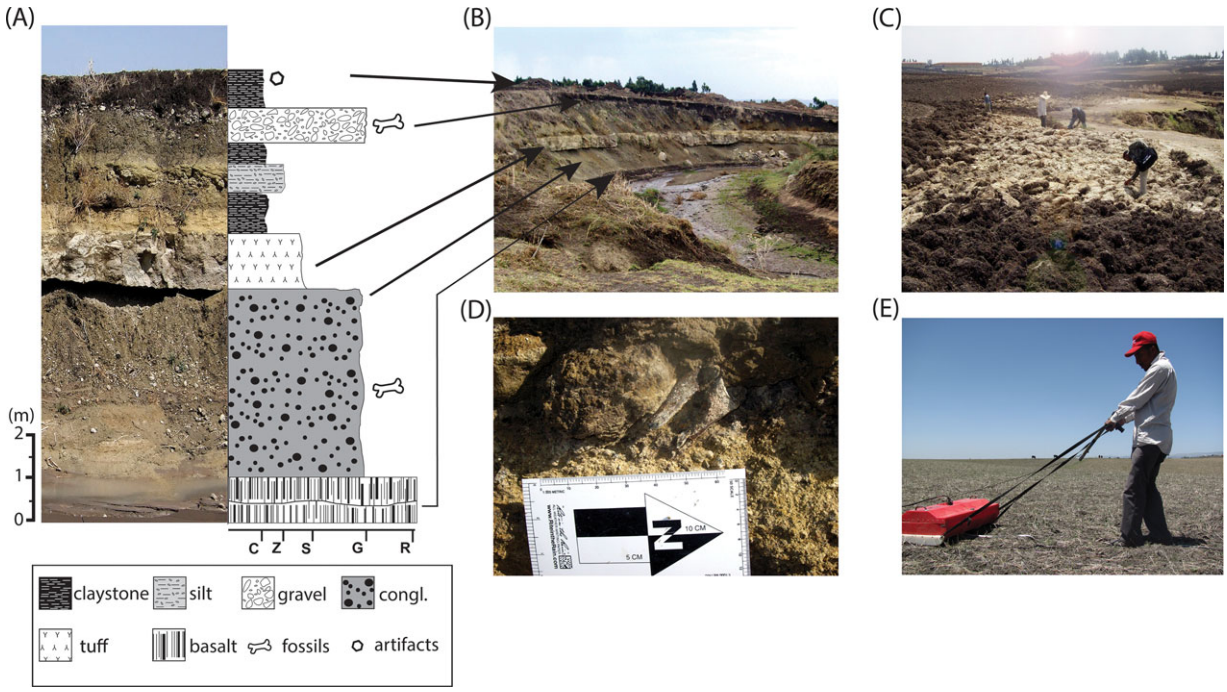

Figure 3 Images from the Fanta Stream site. (A) Type section from the stream cut bank exposure with stratigraphic interpretation. C—clay, Z—silt, S—sand, G—gravel, R—consolidated rock. (B) Elongated view of the cut bank sedimentary exposure at a large meander. (C) Extensively plowed area at Fanta with observable upturned sediments and fossils exposed at the surface (*pictured: local Akaki Government officials investigating the site during GPR fieldwork*). (D) Example of *in situ* fossil material in the conglomerate section. (E) GPR data acquisition illustrating flat surface conditions during the survey (*pictured: Assiged Getahun*).

and magnetic properties that are generated during conditions such as contrasting water content, bulk density, or the lithology of discontinuous surfaces, the result of which are imaged by GPR and is an effect of a material property's relative dielectric permittivity (RDP).

Our investigations at the Fanta Stream site relied on a GSSI SIR-2 single channel control unit and 100 MHz shielded monostatic antenna. To reduce field time over a large spatial extent, the authors determined that a 100 MHz center frequency antenna was an appropriate tool to identify geologic associations in this environment, as the site's initial description and sedimentary observations had taken place in 2008, a year before the acquisition of the first radar survey. Considering the observed surficial claystone and silty tuff units were hypothesized to cause a significant degree of attenuation (e.g., Olhoeft, 1996; Neal, 2004; Zhao et al., 2013), the authors selected a lower operating frequency to overcome energy losses and increase range, where a 250 ns time window was utilized (e.g., Koppenjan, 2009).

We surveyed 19 grids totalling ~17,000 m^2 over the course of 3 weeks in 2009, and infilled and expanded these data in 2010 with a series of two-dimensional lines collected orthogonally to the principal grid orientations from the 2009 survey. Variations in soil–water saturation and surficial conditions inhibited robust ties in the deeper portions of the profiles between the two data sets, and ultimately the 2009 survey data provided the best data quality for stratigraphic interpretation (Lanzarone et al., 2010). Examining all of the GPR data from the two field seasons provides a detailed subsurface description of the site; however, given the objective of this paper is to broadly characterize the stratigraphy away from the exposed cut bank, we ultimately only present selected profiles and slices here (for a comprehensive account of data acquired during both 2009 and 2010 field seasons, see Lanzarone, 2011).

GPR grids were spaced broadly across the site to compare GPR data with the initial site delineation and ultimately to refine the site's boundaries. Various strategies were attempted in adequately sampling geophysical data within and away from the previous site delineation based on fossils and artifacts observed on the site's surface.

The authors acquired the survey employing single-orientation transects at a speed of 1 m/s, where lines were acquired parallel to each other spaced at 0.5 m, a standard acquisition strategy for the 1 m wide 100 MHz

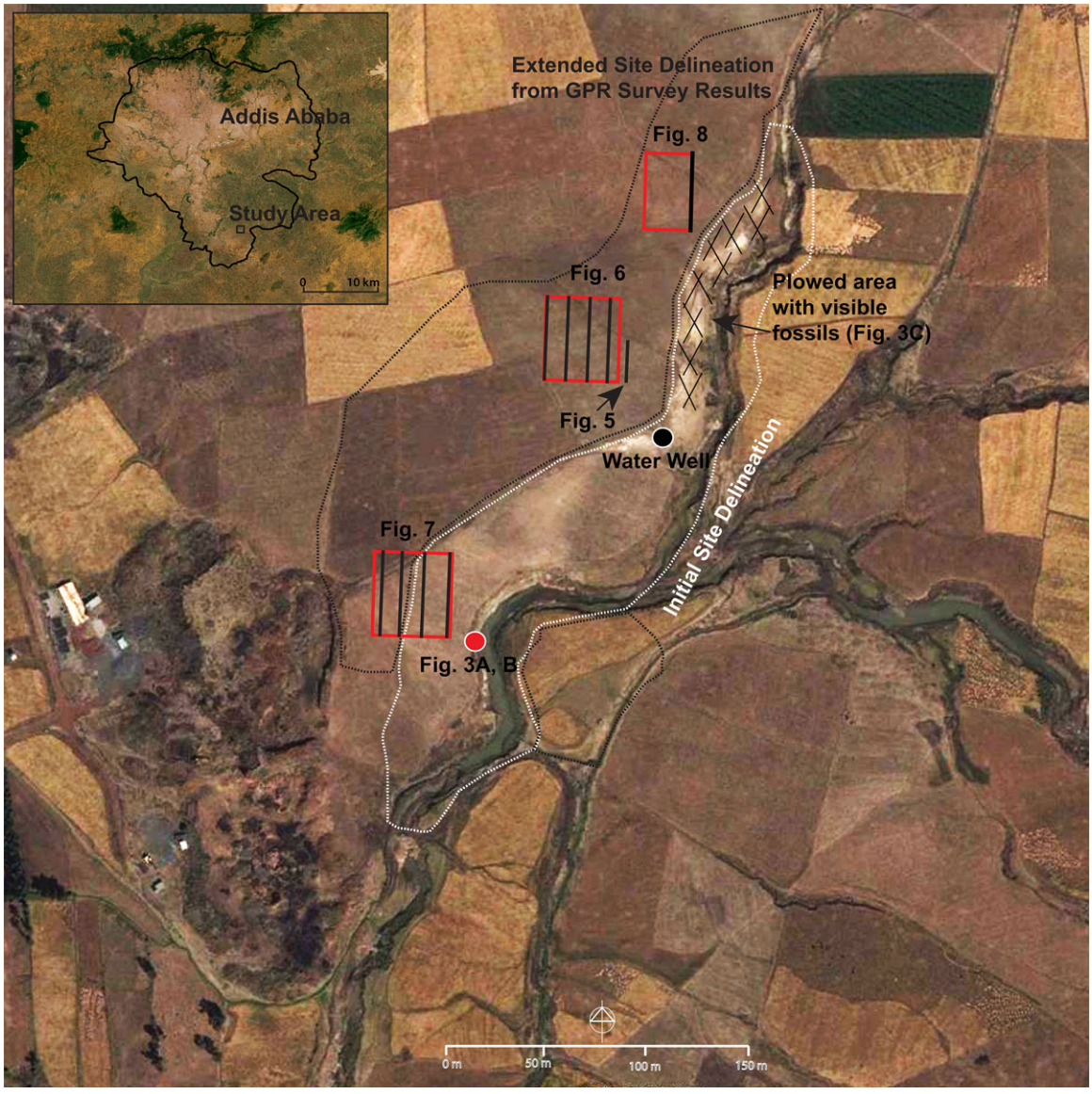

Figure 4 Satellite image outlining detailed locations of GPR profiles, slices, and major features at the site as discussed throughout the text. GPR profiles and grids are referenced by figure numbers adjacent to each line diagram. Source: Google Earth 7.1.2.2041. 2009. Addis Ababa Southeast, 8°52′56.82″N, 38°48′2.48″E, elev. 2.1 km [accessed 20 March 2014].

antenna for geologic targets (Geophysical Survey Systems, Inc., 1995; Jol, 1995). We utilized a sample interval of 512 samples per scan at 32 scans/s. This provided sufficient data density designed for the large-scale survey acquired here and is considered standard for most applications utilizing a 100 MHz antenna (Geophysical Survey Systems, Inc., 1995). All grids were spatially referenced to permanent water well at the site that we use to identify GPR grid and transect locations. We also implemented high-resolution global positioning system to demarcate transect orientations for future identification. Figure 4 outlines the location of selected GPR profiles, depth slices, and other features at Fanta Stream site highlighted throughout this paper.

The authors attempted to acquire hand-augered cores at various locations along with the acquisition of GPR data. Core data could corroborate our GPR interpretation and velocity estimation, and would be useful in providing a ground truth to the interpretation of GPR events far from the stream cut bank where possible variations in moisture and stratigraphic complexity could generate significant lateral velocity variation. Unfortunately, due

to issues related to limitations of field equipment and the impenetrable graveliferous and cobble deposit near the upper ~1 m at the site, we were not able to obtain cores deep enough to shed light on subsurface GPR data.

GPR postacquisition data processing was performed using GPR SLICE v.7 software. Our processing flow followed standard techniques in GPR and reflection seismology processing (Yilmaz, 1987; Cassidy, 2009). Individual profiles were reversed based on data acquisition orientation. Horizontal sampling was applied utilizing hand-marker navigation collected every meter. Manual gain application and time-zero correction of the two-dimensional profiles were performed before the application of background, deconvolution, and band-pass filtering to produce two-dimensional images that we ultimately interpret. Additionally, we applied a Hilbert transform along with the previous processing steps. This process converts radar profiles into positive domain envelopes for ease of visualizing gross stratigraphic packages and the relationship between profiles and slices. We also employ boxcar smoothing on Hilbert transform profiles to smooth high-frequency random noise for better correlation with low-pass filtered amplitude slices. Finally, because of low variability in surface topography, the authors did not employ static corrections on profile data. Figure 5 outlines each step in our processing flow on a single GPR profile.

We calculated an average velocity of 0.09 m/ns based on the correlation of stratigraphic units observed at the Fanta site with GPR profiles. This was done by acquiring transects in the same location as exposed stratigraphy. As outlined in Figure 4, selected profiles presented here are within close proximity to the cut bank exposure, however the authors acquired additional profiles directly along strike of clear exposures visible from the channel axis that exhibit prominent reflection events we observe in virtually every profile.

The most apparent feature is represented as a shallow high RDP contrast event set, giving rise to the top of a distinct series of continuous high-amplitude reflectors seen throughout all of the profiles at the site. Additionally, surface claystones and silty volcanic tuffs were dry to moderately dry during GPR data collection, where velocities from 0.06 to 0.09 could be expected (Neal, 2004; Cassidy, 2009) (for a more comprehensive background on GPR time-depth conversion, please see: Conyers & Lucius, 1996; Sharma, 2002; Conyers, 2004; Neal, 2004; Cassidy, 2009; Goodman et al., 2009; Goodman, 2014). We calculated the vertical resolution of these data at 22.5 cm, the theoretical resolution required to discriminate vertical geologic observations based on the quarter-wavelength approximation (Jol, 1995; Schwamborn et al., 2002).

Amplitude depth slices were generated from profiles using inverse-distance interpolation, and sliced to 5.9 ns (~0.26 m) thick intervals. We also interpolated between slices to generate a three-dimensional slice volume. The selected slice thickness provided 30% overlap between each depth slice from the surface to the maximum usable depth of the survey and satisfied assumptions based on our estimation of vertical resolution. This provided sufficient vertical and spatial sampling to identify lithologic contrasts of submeter scale bed thickness. We applied a low-cut filter to depth slices in order to observe broad amplitude variations across identified intersecting surfaces. This process ultimately reduced acquisition striping seen in some raw slice images. Other methodologies used to reduce striping were considered and tested (e.g., Leckebusch, 2005; Cheyney et al., 2012), however, the best results for these data were generated from the aforementioned processing methodology.

RESULTS

Large areal extent, landscape geophysical surveys are often complex and time consuming to acquire, process, and interpret. Here, we present selected results from three grids surveyed across the Fanta Stream site.

GPR data collected at Fanta reflects high-quality subsurface imaging throughout the three-dimensional surveys we acquired. Noise observed in raw images were filtered during data processing, particularly in the shallow section of the profiles where a high-amplitude direct wave masks usable signal in the upper 0.9 m throughout many of the images (Figure 5A). The authors experimented with background filters (Figure 5B) judiciously to attempt only removing noise from the recorded data. Surficial clay deposits were expected to give rise to signal reverberation (Cassidy, 2009), and were considered throughout our processing workflow. We performed quality control on filtered images using difference displays to examine only data that were removed during the filtering process. Figure 5C shows the result of the background filtered image subtracted from the raw image. In this display, it is clear that only horizontal banding has been removed. Figure 5D shows the image after deconvolution has been applied to the background filtered data. Deconvolution is used to reduce energy of multiple reflection events by converting pulse energy into the spectral domain using a fast Fourier transform, calculating the logarithm of the spectral component, and converting back into the time domain (Goodman, 2014). This had the effect of largely removing unwanted multiples and allowed the authors to have more confidence in our

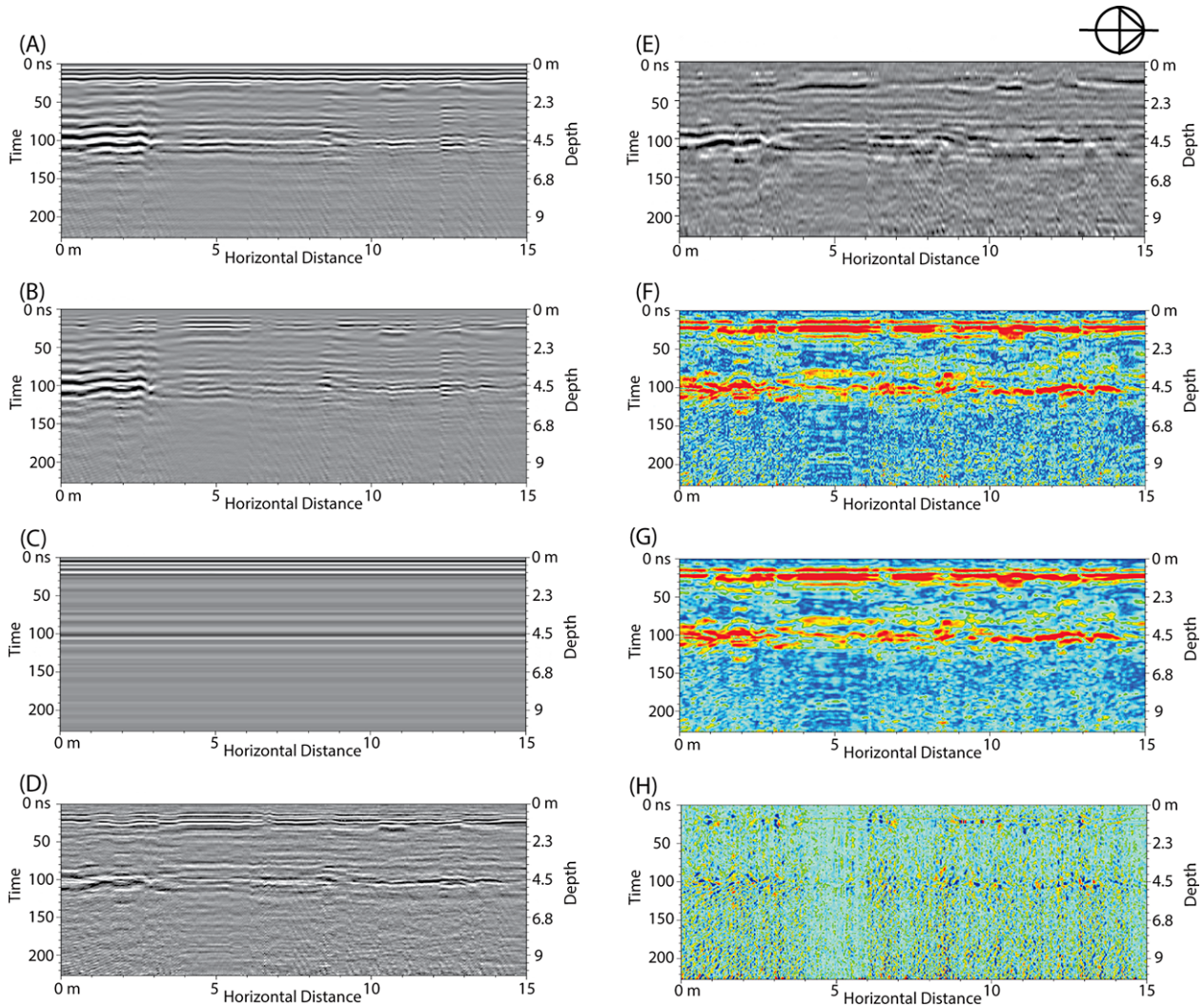

Figure 5 Examples from the postacquisition GPR processing and filtering sequence employed on interpreted data. (A) Raw data. (B) Background removal filter. (C) Difference display of raw and background removal filter. (D) Deconvolution filter. (E) Bandpass filter. (F) Hilbert transform. (G) Hilbert transform with boxcar filter applied. (H) Difference display of Hilbert transform and boxcar filter. Warm colors represent high amplitudes, cold colors represent weak amplitudes.

subsurface interpretation. Comparing with Figure 5B, deconvolution helped to remove multiple energy seen within the first 3 m horizontally across the profile, and provided better focusing of the high-amplitude reflector at ~4 m depth. We applied a band-pass filter in Figure 5E in order to remove high-frequency noise. Some of the signal was inadvertently removed in the uppermost section (0.5–1.4 m), but the overall continuity of the gross event packages are apparent in the shallow section of Figure 5E. Figure 5F shows the addition of applying a Hilbert transform, a process that was used to highlight dominant radar events. We eliminated high-frequency noise using boxcar smoothing (Figure 5G), and show the difference display where much of the vertical noise has been removed in preserving signal (Figure 5H).

Before acquiring these data, it was unknown how GPR would behave in this environment due to expectedly high-attenuation clay soils at the site's surface, commonly thought to pose issues with depth of penetration in certain environments. Despite this, it appears as though useable signal below the shallowest section of the acquired profiles is preserved.

GPR reflection data were reliably obtained to depths up to 9 m in most locations. Data toward the bottom of many profiles were largely attenuated, so the authors ultimately removed deeper sections that did not lend to

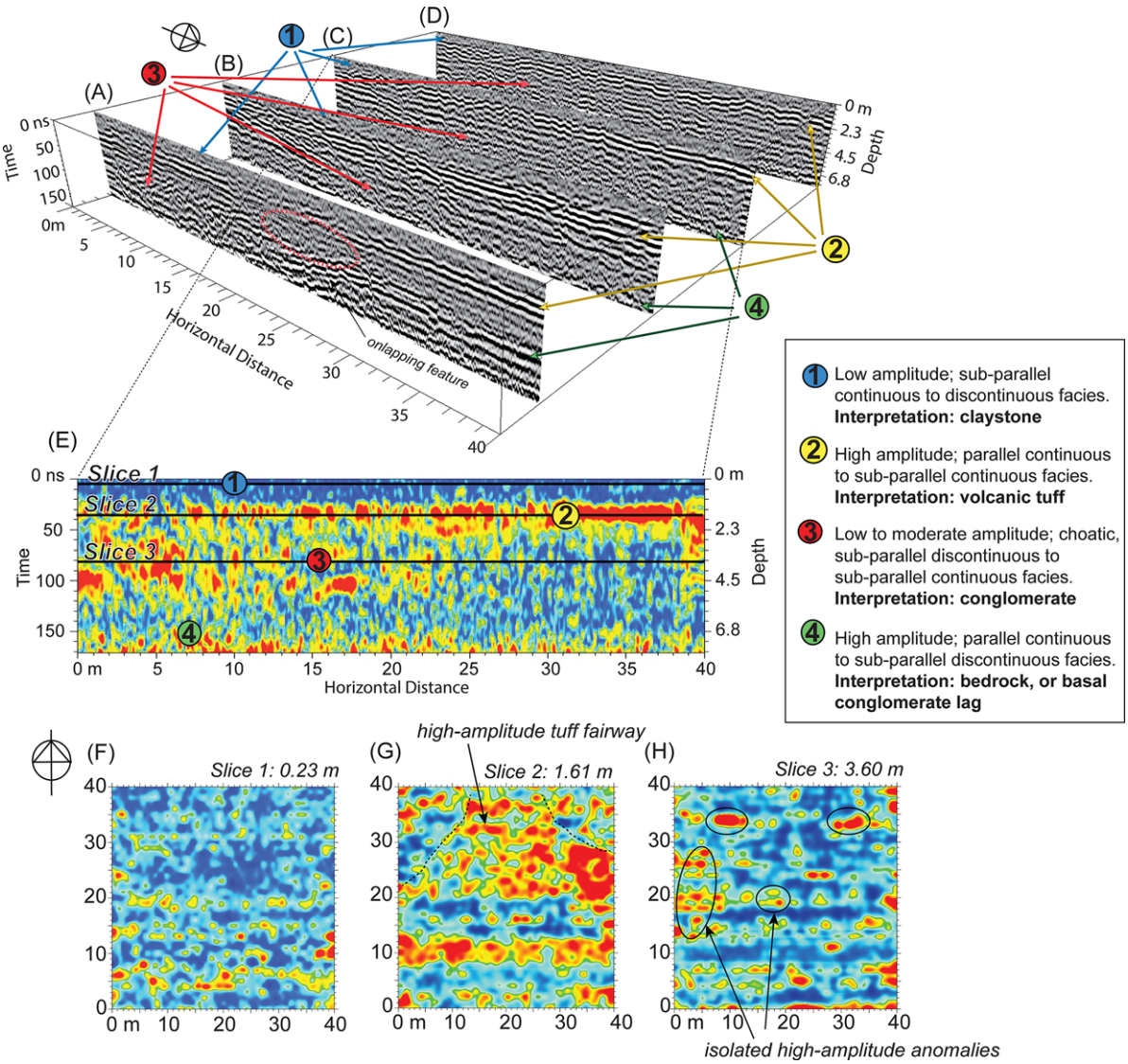

Figure 6 (A–D) Selected adjacent profiles that make up the surveyed GPR grid. (E) Selected GPR profile Hilbert transform display. (F–H) Depth slices with annotations highlighting the authors' interpretation. Warm colors represent high amplitudes, cold colors represent weak amplitudes.

interpretation due to high noise levels and low reflection strength. Signal attenuation at significant depths is clear on the raw profiles (e.g., Figure 5A), where a lack of coherent energy appears at depths greater than 7 m in this image.

We utilize two-dimensional and two-and-one-half-dimensional displays to visualize multiple profiles for comparison of data quality and coherency of observable radar events. Figure 6 shows GPR profiles that were acquired in a 40 × 40 m grid orientation, where the southeast corner of Figure 6A is located approximately 60 m from the stream cut bank. We present interpreted profiles as grayscale variable density (Figure 6A–D), Hilbert transform (Figure 6E), and depth-slice displays (Figure 6F–H) with annotations. We display Figure 7 in a similar manner as Figure 6 to visualize the profiles that span the length of this 40 × 40 m grid, acquired 10 m away from the cut bank in the case of Figure 7D. In Figure 8, we show an intersecting Hilbert transform profile and depth slices to visualize how radar events interpreted in profile view extend laterally at various depth intervals. We display the northernmost grid acquired in this survey utilizing 20 × 40 m spacing at 35 m distance from the stream profile from the southeast grid corner.

We utilize GPR profile and slice data as well as stratigraphic observations from the stream cut bank in

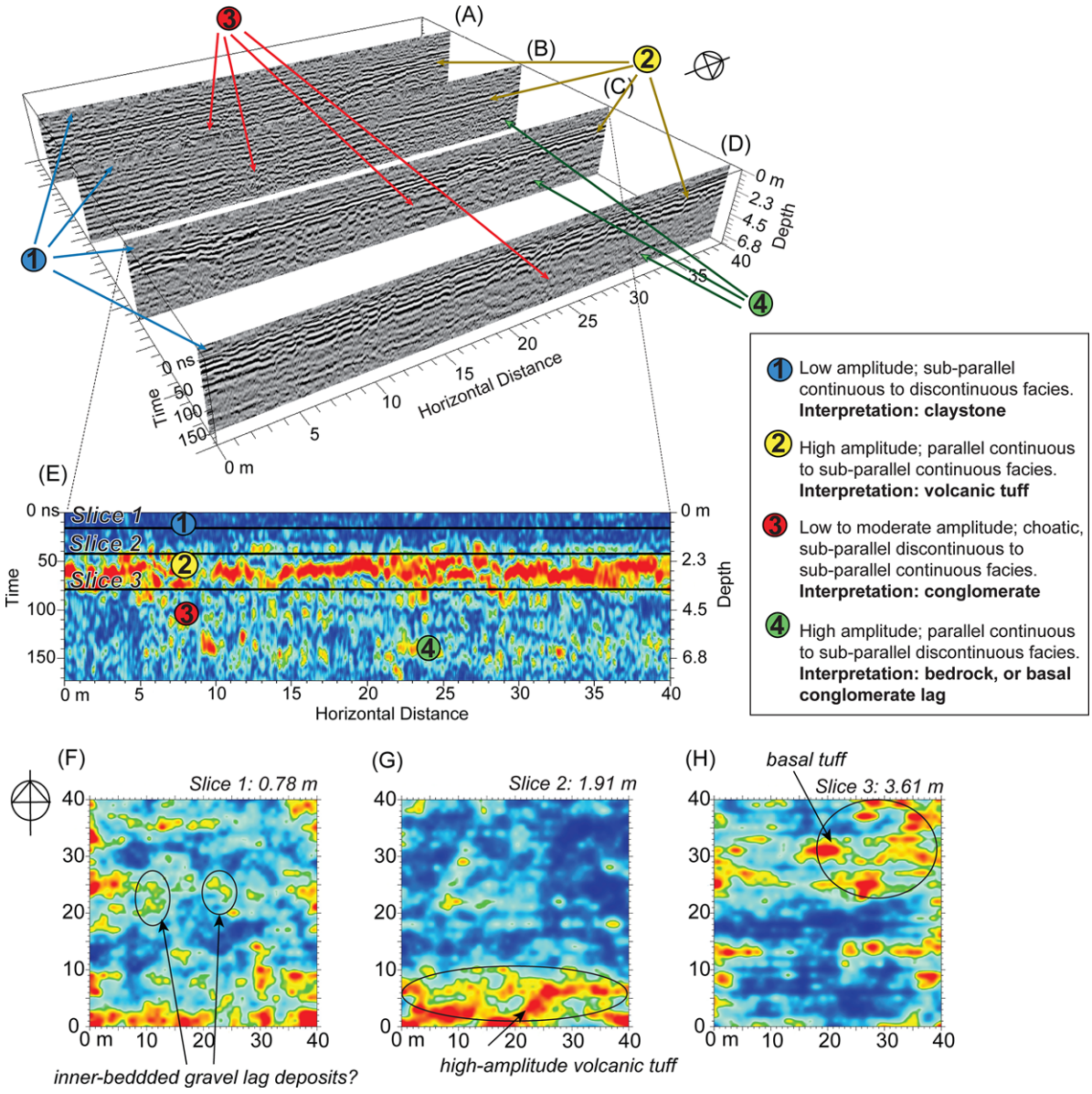

Figure 7 (A–D) Selected profiles from the surveyed GPR grid, southwest of Figure 6. (E) Selected GPR profile Hilbert transform display. (F–H) Depth slices with annotations highlighting the author's interpretation. Warm colors represent high amplitudes, cold colors represent weak amplitudes.

order to identify reflection events spatially and temporally, and devise a subsurface framework with which to interpret the stratigraphy of Fanta away from the cut bank exposure.

INTERPRETATION AND DISCUSSION

Some sedimentary units exhibit distinctive reflection geometries that allow interpreters to group bedforms into various depositional elements (Vandenberghe & van Overmeeren, 1999; Neal, 2004; Gomez-Ortiz et al., 2006). The Fanta Stream's geology is such that clear, well-bounded units exposed along the channel cut bank allow the authors to make direct calibrations to these observed units using geophysical data. We identify four major reflection geometries that are consistent with sedimentary units at the site that we group into GPR facies.

At the top of all GPR profiles, a clay unit exhibits radar facies consistent with relatively low-amplitude, subparallel discontinuous reflections (Facies 1). This is

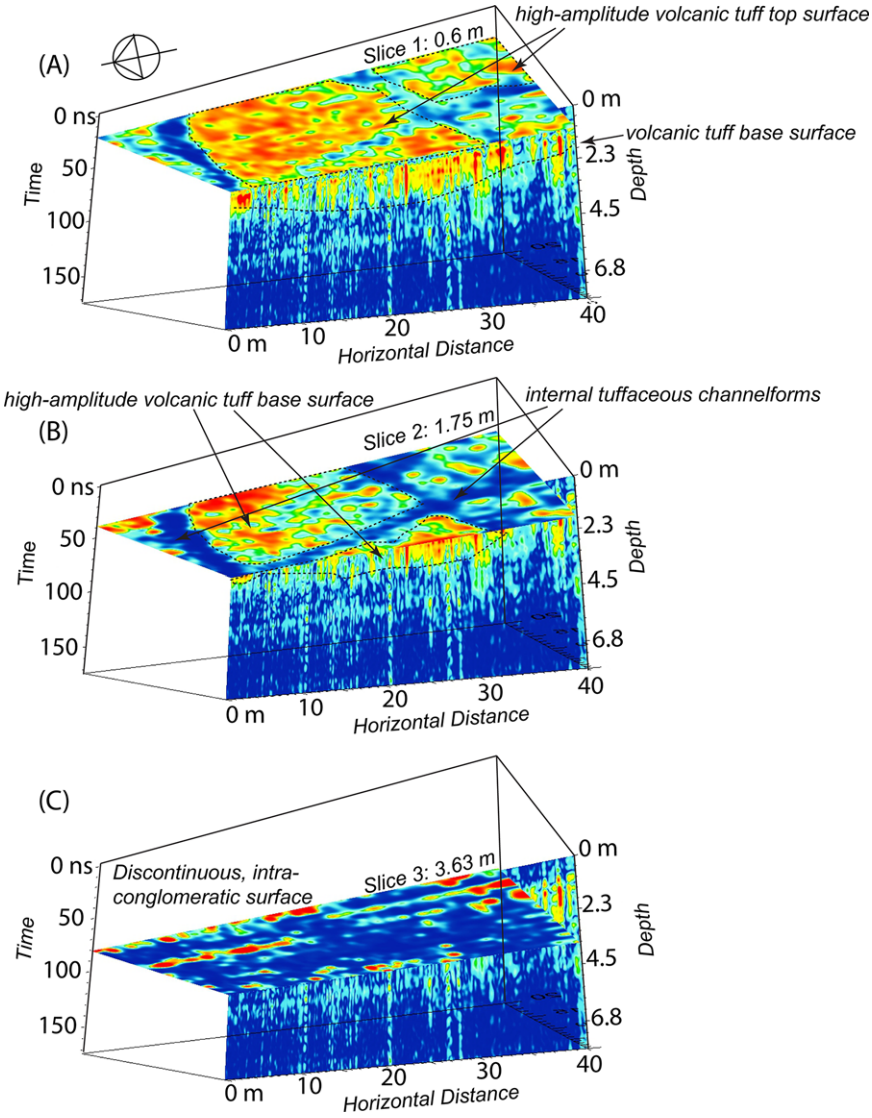

Figure 8 (A–C) Intersecting GPR depth slice at various depth intervals along a vertical profile. This figure highlights the confluence of planar stratified volcanic tuff and incising redeposited tuff deposited by fluvial action as well as deeper conglomeritic material, and relates how radar facies and amplitude depth slices can illuminate the Fanta Stream's paleomeander pattern in the subsurface. Warm colors represent high amplitudes, cold colors represent weak amplitudes.

consistent with the nature of the structureless sedimentological expression of this unit observed in the cut bank exposure and across the surface of the site. Resulting GPR data from this shallow section unfortunately did not allow the authors to confidently discriminate between the deeper fossil-bearing gravel unit and overlying claystone, one of the core objectives of this study. This was likely due to insufficient resolution related to the low-frequency nature of the antenna at this shallow depth as well as the structureless sedimentary fabric of the claystone and the deeper poorly sorted graveliferous unit, giving rise to a diffuse lithologic contrast and thus weak RDP contrast measurable by GPR. Additionally, the shallow section of many profiles is obscured by direct wave interference observed in the raw data when compared with the deeper section.

Depth slices across intervals defined as Facies 1 exhibit minor amplitude variation that may be related to gravel lag deposits with well-defined bedding in contrast to the structureless clays. In Figures 6F and 7F, the authors interpret the weak amplitude segments as clay and the higher amplitude anomalies as gravel lag deposits, which

in general have a greater chance of preserving bedding and reflecting radar energy. Figure 7F shows a more extensive concentration of well-defined isolated amplitude features, suggesting that there may be a greater chance of preserving gravel beds at and near this location compared with Figure 6F, in which the anomalies present in the depth slice appear spottier and less coherent.

Volcanic tuffs are the most readily identifiable and well-recognized facies, as reflection events at this level exhibit a high-amplitude, subparallel to parallel continuous coherent reflection pattern (Facies 2). It was expected that a substantial RDP contrast from the volcanic tuff would cause a significant amplitude response compared with shallower sedimentary units at Fanta. Other case studies from GPR literature have highlighted the response of volcanic ash and pumice beds that manifest as high-amplitude GPR events (e.g., Russel & Stasiuk, 1997; Tohge et al., 1998; Chow, Chang, & Yu, 2006; Rust & Russell, 2000). The facies observations from this unit reflect the thin-bedded to laminated nature of this sedimentary package that was observed in the cut bank exposure. A clear top and base of this high-amplitude section can be tracked across many of the profiles and amplitude depth slices, highlighting the continuity of this subsurface reflection package across the site. Some internal variation within the facies association exists as well, which may reflect subtle dips of interbedded deposits or channeling within the tuffs.

In some areas, the top of the high-amplitude tuff appears deeper, suggesting that the shallower graveliferous unit may thicken elsewhere at the site and could have greater potential for fossil deposition. Comparing Figures 6E and 7E, Facies 1 is ~0.5 m thicker in Figure 7. Additionally, other profiles west of Figure 7C or E show increased thickening of Facies 1 (Figure 7A, B) laterally away from the cut bank.

Depth slices show the lateral expanse of Facies 2, exemplified in Figures 6G, 7G and H, and 8A and B. The curvilinear features observed in the northern high-amplitude section of Figure 6G may indicate that the tuff was deposited in a channel originating to the north of the study area. Additionally, the amplitude variation seen in Figure 7G and H likely indicates a change in dip of the tuffaceous unit, where the highest amplitude segments appear to deepen toward the north. Figure 8A and B show a similar high-amplitude signature interrupted by clear, weaker amplitude curvilinear anomalies. We interpret the anomalies as a paleofluvial meandering pattern within the volcanic tuffs. In sections of the cut bank exposure, we observe pumices and rock fragments deposited in isolated locations that suggest channelization within the tuff.

The deeper, fossil-containing conglomeritic section that contains *in situ* fossils is present below the volcanic tuff unit. Reflection events at this depth interval are largely subparallel discontinuous and chaotic in some areas (Facies 3). This likely reflects the nature of this sedimentary unit, where poor sorting and crude stratification contributes to the overall radar reflection geometry. This appears to be similar to the description of Facies 1, however, the overall weaker continuity and moderate amplitude of reflection events makes this facies distinct.

Figure 6A demonstrates some of the characteristics of internal bedding within Facies 3, where reflectors at ~3.0–4.5 m depth are onlapping deeper high-amplitude dipping events below (from 15 to 25 m along the horizontal axis). This may indicate deeper structural controls from bedrock features and its impact on the overlying conglomeritic deposits. The overall lack of coherency throughout this facies association corresponds to the weakly bedded nature of this lithologic unit and the GPR signal response on both profiles and slices.

In the deepest section of the profiles, relatively high-amplitude, high-reflection strength events make up a high-contrast material hypothesized to be basaltic bedrock (Facies 4). This feature is present in Figures 6 and 7 and ranges from 5.5 to 7 m depth. The facies identified here is consistent with the depth to bedrock observed in the cut bank and is the maximum depth to which the exposed sedimentary deposits containing fossils occur.

Figure 6A exemplifies the high-amplitude nature of Facies 4 at the bottom of the profile at ~5 m depth, and contrasts to the more graded geometry and deeper positioning of this section as we move toward the east of this grid. This may indicate that the bedrock is dipping downward toward the east, having implications that the conglomeritic package may be thickening in this direction. Figure 7E does not show as strong a contrast for Facies 4, and may suggest a breakdown at the interface of sediment and bedrock manifested as a diffused contact, or the nature of increasing signal attenuation with depth in this part of the site.

Using GPR profiles and depth slices as well as integrating the stratigraphic features of exposed sediments allows the authors to formulate a cohesive interpretation of sedimentary facies across the site. Ultimately, the processed GPR data greatly add to the subsurface description at Fanta, which is effective in its ability to image stratigraphic variations away from the cut bank exposure. These data can thus be used to focus excavation areas of probable fossil accumulations, and better outline higher probability zones used to guide future work outboard of previously identified portions of the site.

CONCLUSIONS

The Fanta Stream site shows great promise in yielding valuable information on early hominid and mammalian paleoecology, and could be a critical data point in deciphering the complex chronology of central Ethiopia. Fossil and artifact associations at Fanta allow for a glimpse into hominid activities and behavior during the Acheulean period. The coarse appearance of lithic tools at the site's surface suggest these may date to as far back as 600 ka, and although artifacts were not observed *in situ* within the cut bank exposure, observations from lithics are certainly a component of placing the site into a greater regional context on the movement and behaviors of early hominids in this area. Future work at Fanta will involve excavating and further mapping of fossil deposits and the surrounding strata. Additionally, use-wear analyses on lithics and their association with fossil deposits could help to further the understanding of early hominid behavior patterns during the Acheulean period in central Ethiopia.

By examining GPR depth slices and profiles, our GPR survey allows us to interpret the changing landscape surrounding the Fanta Stream, and place the site into a larger paleoenvironmental context. We observe similar GPR facies distributions consistently throughout our data that we interpret from both two-dimensional profiles and amplitude depth slices. We also tie these data to stratigraphic observations from the stream cut bank.

Results and subsequent interpretation of the GPR survey data extended the overall areal extent of the site by more than double. We show the initial site delineation and expanded area from the GPR survey in Figure 4. Notably, the area toward the west of the modern stream has significant potential for the presence of fossil-containing sedimentary units. For the purposes of this paper to exemplify the 2009 field season from selected GPR data, we examine only a few of the grids and transects used to justify our expanded site extent; however there is a significant amount of additional data from other areas surveyed that have not been captured here (see Lanzarone, 2011). Additionally, it is likely that fossil and artifact accumulations are more expansive than the revised site outline presented in Figure 4. The current map reflects evidence from the area surveyed by GPR but could extend significantly based on additional geophysical data or test excavation units. Considering the delicate balance between continued producing farmland and cultural resource management, the area presented here should be considered the minimum site extent.

The nature of the 100 MHz frequency antenna did not allow for detailed high-resolution imaging of the shallowest stratigraphic boundaries at the site, where we were unable to reconcile contrasts in surficial clays and fossil-rich gravels. However, our observation regarding the varying thickness of this section allows us to recommend the location of expanded areas of possible fossil-containing gravel units. Future work in identifying the shallow fossil-bearing gravel may benefit from conducting a GPR survey utilizing a higher frequency antenna and closer transect spacing. For the purposes of gross characterization of the site and imaging the deeper volcanic tuff, conglomerate, and bedrock, the 100 MHz antenna ultimately provided sufficient resolution.

This paper highlights the efficacy of GPR for paleontological reconnaissance through stratigraphic radar facies interpretation. The furthered use of this technology could be beneficial in exploring fossil deposits elsewhere in Eastern Africa and in other parts of the world. It is hoped that in the future, the Fanta Stream site will be a high-priority fossil and archaeological locale in which to conduct excavations and utilize for student and public education. The GPR study conducted here has shed light on high-priority excavation areas once this project is sanctioned for protection and full-blown archaeological excavatory work.

The authors would like to thank the local residents of Akaki and Addis Ababa for their support and participation in this field research. We are particularly grateful to Jara Haile Miriam, Yonas Beyene, Mogus Mekonnen, Ayele "Butu" Desta, Mohammed Umer Mohammed, Enqu Wondimu, and Ato Kostentinos. We would also like to give a special thanks to the various individuals who assisted in the development of this paper, including Zelalem Assefa, Chris Lepre, Rob Hawman, Nathan Mountjoy, Kent Schneider, Dean Goodman, William Bunting, Daniel Bigman, Steven Brandt, and Erich Fisher. Funding was provided by The Geological Society of America Student Research Grant, Grant-In-Aid of Research from Sigma Xi, The Scientific Research Society; Claude C. Albritton Jr. Memorial Student Research Award; Geological Society of America Graduate Student Travel Grant; Joseph W. Berg Scholarship; The University of Georgia Student Association for Archaeological Sciences Small Grant; and the Miriam Watts-Wheeler Scholarship; without which none of this research would have been possible. Finally, we are grateful to Editors Jamie Woodward and Gary Huckleberry as well as Barry Taylor and the anonymous reviewers for their helpful and constructive comments which significantly improved this manuscript.

REFERENCES

Abebe, T., Mazzarini, F., Innocenti, F., & Manetti, P. (1998). The Yerer-Tullu Wellel volcanotectonic lineament: A transtensional structure in central Ethiopia and associated magmatic activity. Journal of African Earth Sciences, 26, 135–150.

Abebe, T., Balestrieri, M., & Bigazzi, G. (2010). The central main Ethiopian Rift is younger than 8 Ma: Confirmation through apatite fission-track thermochronology. Terra Nova, 22, 470–476.

Adhana, T. (2014). The occurrence of a complete continental rift type of volcanic rocks suite along the Yerer-Tullu Wellel Volcano Tectonic Lineament, Central Ethiopia. Journal of African Sciences, 99, 374–385.

Amante, C., & Eakins, B. (2009). ETOPO1 1 arc-minute global relief model: Procedures, data sources and analysis. NOAA Technical Memorandum NEDIS NGDC-24. National Geophysical Data Center, NOAA, Washington D.C.

Awulaachew, S., Yilma, A., Loulseged, M., Loiskandl, W., & Alamirew, T. (2007). Water resources and irrigation development in Ethiopia. Colombo, Sri Lanka: International Water Management Institute.

Boccaletti, M., Bonini, M., Mazzuoli, R., Abebe, B., Piccardi, L., & Tortorici, L. (1998). Quaternary oblique extensional tectonics in the Ethiopian Rift (Horn of Africa). Tectonophysics, 287, 97–116.

Cassidy, N. (2009). Ground penetrating radar data processing, modeling and analysis. In H. Jol (Ed.), Ground penetrating radar: Theory and applications (pp. 141–172). Oxford: Elsevier.

Cheyney, S., Hill, I., Linfod, N., & Fishwick, S. (2012). New approach to directional filtering of near-surface magnetic data. Near Surface Geophysics, 10, 359–367.

Chow, J., Chang, S., & Yu, H. (2006). GPR reflection characteristics and depositional models of mud volcanic sediments-Wushanting mud volcano field, southwestern Taiwan. Journal of Applied Geophysics, 60, 179–200.

Conyers, L. (2004). Ground-penetrating radar for archaeology. Walnut Creek, CA: Altamira Press.

Conyers, L., & Lucius, J. (1996). Velocity analysis in archaeological ground-penetrating radar studies. Archaeological Prospection, 3, 25–38.

Garrison, E. (2003). Techniques in archaeological geology. Berlin: Springer-Verlag.

Geophysical Survey Systems, Inc. (GSSI). (1995). SIR SYSTEM-2 training notes. New Salem, NH: GSSI (unpublished). http://www.geophysical.com/Documentation/Manuals/SIR2Manual.pdf.

Getahun, A. (2007). Geology of Addis Ababa City. Unpublished Report. Addis Ababa: Office of the Ministry of Mines and Energy Regional Geology and Geochemistry Department, Addis Ababa, Ethiopia.

Gomez-Ortiz, D., Matrin-Velazquez, S., Martin-Crespo, T., Marquez, A., Lillo, J., Lopez, I., & Carreno, F. (2006). Characterization of volcanic materials using ground penetrating radar: A case study at Teide volcano (Canary Islands, Spain). Journal of Applied Geophysics, 59, 63–78.

Goodman, D. (2014). GPR SLICE User's Manual Version 7.0. Unpublished Instructional Manual. Gypsy Lane, CA: Geophysical Archaeometry Laboratory. http://www.gpr-survey.com/gprslice/subscribersonly.html.

Goodman, D., Piro, S., Nishimura, Y., Schneider, K, Hongo, H., Higashi, N., Steinberg, J., & Damiata, B. (2009). GPR archaeometry. In H. Jol (Ed.), Ground penetrating radar: Theory and applications (pp. 479–509). Oxford: Elsevier.

Hailemariam, K. (1999). Impact of climate change on the water resources of Awash River Basin, Ethiopia. Climate Research, 12, 91–96.

Jol, H. (1995). Ground penetrating radar antenna frequencies and transmitter powers compared for penetration depth, resolution and reflection continuity. Geophysical Prospecting, 43, 693–709.

Koppenjan, S. (2009). Ground penetrating radar systems and design. In H. Jol (Ed.), Ground penetrating radar: Theory and applications (pp. 73–98). Oxford: Elsevier.

Kvamme, K. (2003). Geophysical surveys as landscape archaeology. American Antiquity, 68, 435–457.

Lanzarone, P. (2011). Ground penetrating radar (GPR) examinations at the Fanta Stream fossil and archaeological site, Central Ethiopia. Unpublished master's thesis, The University of Georgia, Athens, GA. http://athenaeum.libs.uga.edu/xmlui/handle/10724/27202.

Lanzarone, P., Garrison, E., & Getahun, A. (2010). Multi-seasonal ground-penetrating radar (GPR) analyses at the Fanta Stream fossil and archaeological site, Central Ethiopia. 2010 Annual Meeting. Denver, CO: Geological Society of America.

Leckebusch, J. (2005). Use of antenna arrays for GPR surveying in archaeology. Near Surface Geophysics, 3, 109–113.

Leclerc, R., & Hicken, E. (1997). The internal structure of scrolled floodplain deposits based on ground-penetrating radar, North Thompson River, British Columbia. Geomorphology, 21, 17–38.

Main, D., & Hammond, W. (2003). The application of ground penetrating radar as a mapping technique at vertebrate fossil excavations in the Cretaceous of Texas. Cretaceous Research, 24, 335–345.

Neal, A. (2004). Ground-penetrating radar and its use in sedimentology: principles, problems and progress. Earth-Science Reviews, 66, 261–330.

Olhoeft, G. (1996). Application of ground penetrating radar. In Proceedings of the 6th International Conference on Ground-Penetrating Radar. Sendai, Japan.

Patidar, A., Maurya, D., Thakkar, M., & Chamyal, L. (2007). Fluvial geomorphology and neotectonic activity based on field and GPR data, Katrol hill range, Kachchh, Western India. Quaternary International, 159, 74–92.

Russel, J., & Stasiuk, M. (1997). Characterization of volcanic deposits with ground-penetrating radar. Bulletin of Volcanology, 58, 515–527.

Rust, A., & Russell, J. (2000). Detection of welding in pyroclastic flows with ground penetrating radar: Insights from field and forward modelling data. Journal of Volcanology and Geothermal Research, 95, 23–34.

Sagri, M., Bartolini, C., Billi, P., Ferrari, G., Benvenuti, M., Carnicelli, S., & Barbano, F. (2008). Latest Pleistocene and Holocene river network evolution in the Ethiopian Lakes Region. Geomorphology, 94, 79–97.

Schwamborn, G., Dix, J., Bull, J., & Rachold, V. (2002). High-resolution seismic and ground penetrating radar-geophysical profiling of a thermokarst lake in the western Lena Delta, Northern Siberia. Permafrost and Periglacial Processes, 13, 259–269.

Segele, Z., & Lamb, P. (2005). Characterization and variability of Kiremt rainy season over Ethiopia. Meteorology and Atmospheric Physics, 89, 153–180.

Sharma, P. (2002). Environmental and engineering geophysics. Cambridge: Cambridge University Press.

Skelly, R., Bristow, C., & Ethridge, F. (2003). Architecture of channel-belt deposits in aggrading shallow sandbed braided river: The lower Niobrara, northeast Nebraska. Sedimentary Geology, 158, 249–270.

Słowik, M. (2010). Changes of river bed pattern and traces of anthropogenic intervention: The example of using GPR method (the Obra River, western Poland). Applied Geography, 31, 784–799.

Tohge, M., Karube, F., Kobayashi, M., Tanaka, A., & Ishii, K. (1998). The use of ground penetrating radar to map an ancient village buried by volcanic eruptions. Journal of Applied Geophysics, 40, 49–58.

Vandenberghe, J., & van Overmeeren, R. (1999). Ground penetrating radar images of selected fluvial deposits in the Netherlands. Sedimentary Geology, 128, 245–270.

Wright, D., Thompson, J., MacKay, A., Welling, M., Forman, S., Price, G., Zhao, J., Cohen, A., Malijani, O., & Gomani-Chindebvu, E. (2014). Renewed geoarchaeological investigations of Mwanganda's village (elephant butchery site), Karonga, Malawi. Geoarchaeology, 29, 98–120.

Yilmaz, O. (1987). Seismic data processing. Tulsa, OK: Society of Exploration Geophysics.

Yitbarek, A., Razack, M., Ayenew, T., Zemedagegnehu, E., & Azagegn, T. (2012). Hydrogeological and hydrochemical framework of Upper Awash River basin, Ethiopia: With special emphasis on inter-basins groundwater transfer between Blue Nile and Awash Rivers. Journal of African Earth Sciences, 65, 46–60.

Zhao, W., Tian, G., Wang, B., Forte, E., Pipan, J., Lin, J., Shi, Z., & Li, X. (2013). 2D and 3D imaging of a buried prehistoric canoe using GPR attributes: A case study. Near Surface Geophysics, 11, 457–464.

